Title

Investigation of Blade Vortex Interaction Noise Reduction with Leading-Edge Serrations Using High-Fidelity Numerical Simulations

Journal
Vertical Flight Society 81st Annual Forum and Technology Display

Authors
Tran, Huy
Lee, Seongkyu

Publication Date
2025-05-20

DOI
10.4050/f-0081-2025-173

Investigation of Blade Vortex Interaction Noise Reduction with Leading-Edge Serrations Using High-Fidelity Numerical Simulations

Huy Tran
PhD Student

Seongkyu Lee
Professor

Department of Mechanical and Aerospace Engineering
University of California, Davis
Davis, California, 95616 U.S.A.

ABSTRACT

Blade–vortex interaction (BVI) noise primarily occurs in rotorcraft when tip vortices generated by the blades interact with other blades. When BVI noise occurs, it dominates at mid and high blade passing frequency harmonics. To mitigate BVI noise, we employ leading-edge serrations on the OLS rotor between 75% blade span and the tip. High-fidelity computational fluid dynamics simulations, using delayed detached eddy simulation, combined with an acoustic analogy, are conducted to analyze various leading-edge serration geometries with different serration height and wavelength parameters. The results show that rotor BVI noise is reduced by up to 5 dB at the rear of the vehicle when serrations are applied, with higher serration height-to-wavelength ratios proving more effective. The findings demonstrate that when vortices directly impinge on the rotor blades, the serrations disrupt the vortices and generate a fluctuating pressure field on the blade surface, leading to destructive phase interference at the far-field microphone locations.

INTRODUCTION

Rotorcraft noise, particularly that generated by the interaction between rotor blades and vortices, remains a significant challenge in both military and civilian aviation applications. Blade-Vortex Interaction (BVI) noise, a dominant source of sound generated by helicopters and other rotorcraft, has been extensively studied due to its impact on acoustic signatures, which influence both environmental noise pollution and stealth capabilities in military operations (Refs. 1–4). As urban air mobility (UAM) concepts evolve and the demand for quieter and more efficient rotorcraft increases, the need for innovative noise reduction techniques becomes increasingly critical (Refs. 5–9).

Active flow control is one approach to mitigate BVI noise. Using large eddy simulation (LES), Ilie (Ref. 10) injects a jet stream of air at the leading edge of a NACA 0012 airfoil to influence the vortex breakdown event. Typically, stream injections are used to reinforce the boundary layer and delay boundary layer separation, as shown by the reduction in lift and drag coefficients in the conference paper. Applying the leading edge air mass injection to the simulation resulted in a slight increase in sound pressure levels (SPL), but the fluctuation in SPL levels are reduced during BVI events, indicating a reduction in BVI noise. While this may be an effective method for lower BVI noise, further investigation is required to determine the tradeoff for an increase in power expended.

Presented at the Vertical Flight Society 81st Annual Forum & Technology Display, Virginia Beach, Virginia, May 20–22, 2025.

Among the various methods explored to mitigate BVI noise, the application of serrations on the leading edge of rotor blades could be a promising approach (Ref. 11). While serrated leading edges have been extensively studied for their effectiveness in reducing broadband noise on airfoils (Ref. 12), their application to rotor BVI noise remains relatively underexplored. The limited research in this area suggests both a gap in the literature and an opportunity for significant innovation. One notable study by Feinerman et al. (Ref. 13) provides experimental evidence of the potential of leading-edge serrations in reducing BVI noise. In their work, they simulated a BVI event using a controlled gust disturbance nozzle, which generated sudden changes in induced velocity and blade loading as the blades rotate. Their experiments demonstrated a 3 dB reduction in noise in the primary noise propagation direction, attributing this reduction to the phenomenon of phase cancellation. Despite this promising result, there has been little progress on the computational front in terms of modeling BVI noise reduction using serrations, highlighting a critical area for further research.

The mechanisms by which leading-edge serrations reduce BVI noise are multifaceted. First, serrations can modify the flow field around the rotor blade as it approaches and interacts with a vortex. The serrated edges can disrupt the coherence of the vortex by inducing small-scale turbulence, creating multiple, less organized vortical structures. This disruption can diminish the intensity of the primary vortex, leading to a reduction in the pressure fluctuations experienced by the blade. As a result, the noise generated by the interaction can be less abrupt and intense, contributing to an overall reduction in BVI noise.

Additionally, while the primary effect of leading-edge serrations is on the flow at the blade's leading edge, these modifications can also influence the formation and evolution of blade tip vortices. By altering the flow characteristics upstream, serrations can change the downstream development of these vortices, making them less coherent and therefore less likely to cause strong BVI events during subsequent blade passages. This indirect effect further contributes to the noise reduction potential of serrated leading edges. Finally, in terms of sound propagation, the different pressure phases along the serrated edge or in the chordwise direction can contribute to destructive interference in the far field. All these potential noise reduction mechanisms have not been thoroughly studied in the past.

This study aims to leverage high-fidelity computational fluid dynamics (CFD) to rigorously investigate the effectiveness of leading-edge serrations in mitigating rotor BVI noise. By employing advanced CFD techniques, this research seeks to quantitatively assess the noise reduction capabilities of various serrated blade designs and to elucidate the underlying physical mechanisms responsible for BVI noise reduction when using serrated leading edges. The outcomes of this study are anticipated to significantly contribute to the development of quieter rotorcraft, thereby supporting broader objectives related to noise pollution reduction and enhancing the environmental sustainability of aviation technologies.

METHODS

1. Modeling and Flowfield Set Up

In our study, we select the OLS rotor to investigate the rotor BVI noise. The OLS rotor is a scaled model based on the AH-1S helicopter rotor, specifically designed to investigate aerodynamic characteristics during descent flight. The model features a rotor diameter of 1.916 meters, with slight modifications in thickness and chord relative to the full-scale design to facilitate the integration of surface-pressure transducers. A summary of the key rotor parameters is provided in Table 1 and the operating condition is given in Table 2. Further details regarding the airfoil sections, as well as the blade chord and twist distributions, are available in (Ref. 14).

Table 1: Main rotor characteristics (Ref. 14).

AH-1/OLS model rotor	
Radius	0.958 m
Chord length	0.104 m
Twist	10°
Solidity	0.056
Number of blades	2
Airfoil	modified BHT 540 (t/c = 9.71%)
Hinge	teeter type
Tip planform	rectangular

The dynamic motion of the rotor blades is controlled by swashplate actuators, which govern the blade's pitch and flap

Table 2: Operating condition (Ref. 14).

Hover tip Mach number	0.664
Forward speed	72.0 kts
Advance ratio	0.164
Rotor thrust coefficient	0.0054
Shaft inclination angle	2.0 deg (+ aft.)

dynamics through cyclic blade control. The blade pitch angle and blade flap angle are defined by the following cyclic blade pitch and cyclic blade flap equations, evaluated at the 75% blade span location:

$$\theta_{75} = 6.14 - 0.9\cos\psi - 1.39\sin\psi \qquad (1)$$

$$\beta = 0.5 - 1.0\cos\psi \qquad (2)$$

In accordance with the parameters used by Boxwell et al. (Ref. 14) during run 3020, the OLS rotor was tested with an advance ratio of 0.164, an advancing-tip Mach number of 0.773, and a tip-path-plane angle of 2°.

To investigate the impact of leading-edge serrations on noise reduction, the airfoil sections from 75% blade span to the tip of the blade are modified to generate a sinusoidal pattern along the leading edge. The key parameters governing the serration geometry are the height ($2h$), wavelength (λ), and refinement as shown in Fig. 1. The height is defined as the maximum deviation from the reference chord, the wavelength is defined as one period of the sine wave, and the refinement is characterized by the number of airfoil sections per wavelength.

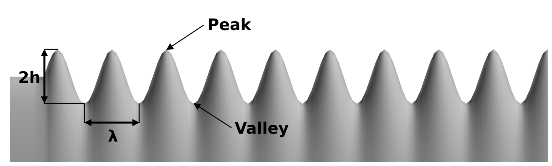

Fig. 1: Serration geometry at the leading edge.

Nine different serration geometries were generated and used for this paper as depicted by Fig. 2. Serrated cases are denoted by two suffix, the first referring to the height-to-chord ratio and the second referring to the height-to-wavelength ratio.

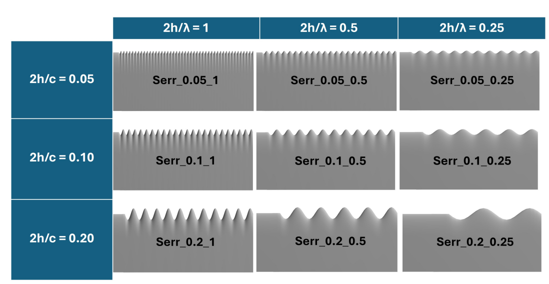

Fig. 2: Serration geometry test matrix.

2. CFD Meshing and Set Up

NASA's Overgrid is employed to generate structured grids. Overgrid facilitates the creation of structured, multi-block grids, which are well-suited for capturing the intricate details of complex configurations. Notably, Overgrid supports the generation of overset grids, also known as Chimera grids, which are essential for simulating moving components like rotating blades and control surfaces by overlapping grids in different regions of the computational domain. In this study, an O-type near-body grid is generated, conforming to the blade shape, which includes the blade, root cap, and tip cap. These near-body grids are overlapped with Cartesian off-body grids. For the baseline case, the grid resolution around the airfoil consists of 277 points along the chord, 100 points in the spanwise direction, and 100 points in the normal direction. Serrated cases had varying spanwise points based on the amount of serrations present and 150 points in the normal direction for better stretching ratio values. To ensure accurate boundary layer resolution, the wall spacing is set to 1.38×10^{-6} m, achieving a dimensionless wall distance (y^+) of 1.0. Surface grids are clustered at the leading and trailing edges in the chordwise direction to resolve large pressure gradients effectively, and similarly along the spanwise direction at the root and tip regions. The near-body volume grids extend up to 1.0 times the reference chord length (C_{ref}) in the wall-normal direction, with the final grid spacing at this boundary with 5% C_{ref}. C_{ref} is defined as the chord length at 75% blade radius. The total number of near-body volume grid points for each rotor blade is approximately 7.1 million, leading to a total of 14.2 million grid points for the baseline OLS rotor system.

For the off-body mesh, a Cartesian grid is automatically generated by the OVERFLOW solver. The off-body grid includes eight levels of refinement, with a fixed refinement box is established around the rotor to resolve and capture tip vortices and wake structures near the blades. The spacing within this refinement box is set to 5% C_{ref}, matching the outer boundary spacing of the near-body grids. The dimensions of the refinement box are 1.25 rotor radii in both x- and both y-directions, 0.3 rotor radii in the positive z-direction, and 0.2 rotor radii in the negative z-direction. The off-body grid contains approximately 32.1 million grid points. The overall domain size for the off-body grid extends 20 rotor radii from the origin in every direction, ensuring that far-field effects are adequately captured. Table 3 shows the detailed number of grid points and computational costs. Figure 3 shows the CFD mesh featuring the overlapping meshes between near-body and off-body grids, as well as grid refinement regions.

NASA's OVERFLOW is utilized for high-fidelity CFD simulations in this study. OVERFLOW is a CFD solver that employs structured, overset grids to solve the compressible Navier-Stokes equations across a wide range of aerospace applications, particularly excelling in simulating unsteady, turbulent flows around complex geometries. The solver adopts a finite-difference approach, supporting both Reynolds-Averaged Navier-Stokes (RANS) models for turbulent flows and Delayed Detached Eddy Simulation (DDES) for capturing large-scale turbulence structures. In the current paper, the governing equations are discretized using a fifth-order central differencing scheme. A second-order scheme is used for viscous flux. As mentioned in the grid generation, the implemented refinement box captures high vorticity, shocks, or other critical flow features in regions of interest. For temporal discretization, a second-order diagonalized Beam-Warming penta-diagonal scheme is employed alongside dual-time stepping subiterations. The maximum number of subiterations is set to 100, allowing the solver to come close to the desired two order of residual drop. A fully turbulent flow condition is simulated in this study using the Spalart-Allmaras 1-equation turbulence model implemented with the

Table 3: Computational size and cost.

Near-body grid	**Baseline**	**Serr_0.1_1**
Blade	2.7 mil	15.6 mil
Tip Cap	2.2 mil	1.0 mil
Root Cap	2.2 mil	2.6 mil
Off-body grid		
	32.1 mil	32.1 mil
Total grid		
	46.3 mil	70.5 mil
Number of processors	384	384
Simulation time per rotor (h)	91.1	146

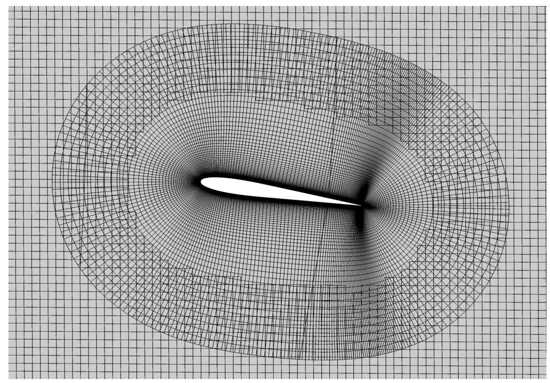

(a)

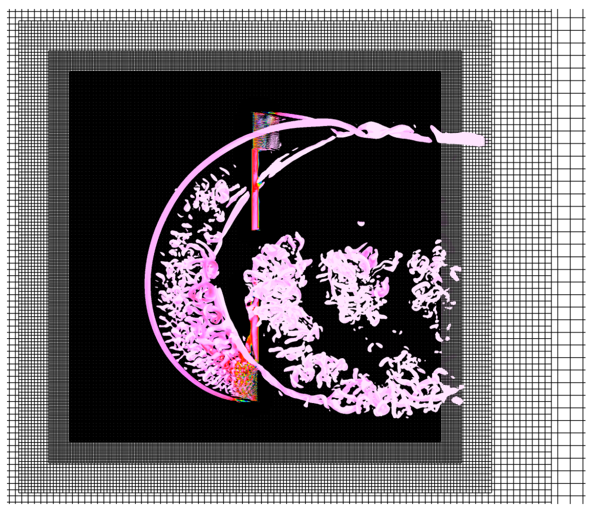

(b)

Fig. 3: CFD mesh: (a) an overlap between rotor near-body meshes and a Cartesian off-body mesh and (b) Cartesian off-body mesh along with the vorticity magnitude.

DDES option. A rotation curvature correction model is also integrated into the fully turbulent simulations to enhance accuracy in predicting vortex flows. The time-accurate simulations are divided into two stages. The initial run uses a timestep size of 0.25° azimuth for 10,080 timesteps, corresponding to 7 rotor revolutions. All CFD simulations were conducted on the UC Davis High-Performance Computing (HPC) system, utilizing 6 nodes with a total of 384 cores. Table 3 outlines the computational resources and costs associated with these simulations.

3. Microphone and Acoustics Set Up

The model OLS test derives its acoustics measurements from the 19 microphones distributed around the wind tunnel. Nine microphones placed in the wind tunnel flow are designated to match and validate corresponding acoustic signatures from the full-scaled experiment AH-1 helicopter. Additional microphones placed outside the wind tunnel flow are used to map the directivity of noise in the far field. Figure 4 shows the in-flow microphones that record near-field acoustic effects and is used to validate the basecase simulation. In the case of this high-fidelity simulation, microphones in-plane to the rotor disk are ignored as these acoustic signatures are more relevant to thickness noise from the geometry and motion of the rotor blades. Instead, we focus on a microphone directly in front of the OLS rotor at a 30° elevation which captures the BVI noise generated by the advancing side. We mirror this microphone in order to capture the acoustics at the rear, capturing the effects from the retreating side. These two microphones cover near field acoustics for the baseline and serrated cases. Figure 5 shows an array of microphones on the side view to visualize the noise directivity. These microphones are placed in a circular pattern with 10 rotor radii and 6° increments, resulting in 60 microphones in total. Noise is predicting using PSU-WOPWOP (Ref. 15). This software solves the Ffowcs Williams and Hawking (FW-H) equation (Ref. 16) using Farassat's Formulation 1A (Refs. 17, 18), yielding the acoustic signature in the time domain. Additionally, PSU-WOPWOP has the capabilities to transform the data into the frequency domain to obtain SPL in the frequency domain.

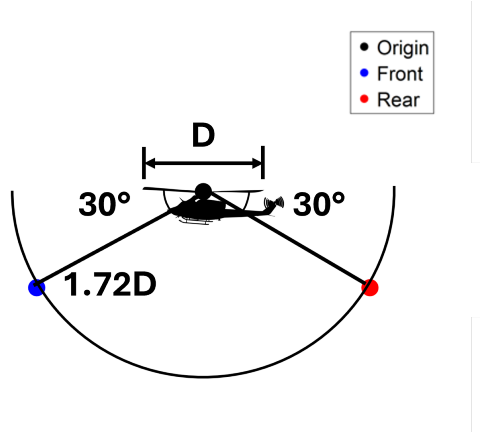

Fig. 4: Near field microphone locations.

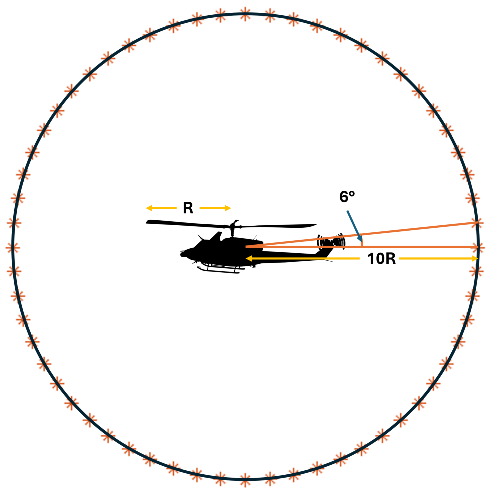

Fig. 5: Far field microphone locations: side view.

RESULTS

1. BVI Aerodynamics

The baseline and serrated leading-edge cases are analyzed for their acoustic performance. We choose $2h = 0.1C_{\text{ref}}$ and $\lambda = 0.1C_{\text{ref}}$, resulting in $2h/c = 0.1$ and $2h/\lambda = 1$ for case Serr_0.1_1. 12 airfoil sections are used per serration to capture the shape of the sinusoidal wave without consuming an excessive amount of grid points.

Figure 6 presents the iso-surface of the Q-criterion for the baseline case, with the non-dimensional vorticity magnitude represented by color. BVI is observed on both the advancing and retreating sides of the rotor. On the advancing side, the tip vortex passes over the blade, while on the retreating side, a direct impingement of the tip vortex onto the blade occurs. Following this direct impingement in the retreating BVI, the vortex breaks down into smaller vortices, contributing to a more turbulent or vortical flow field.

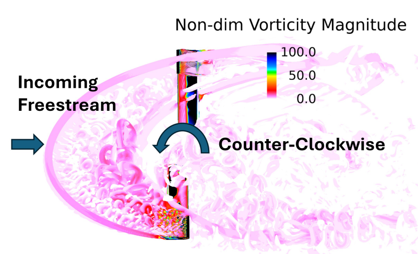

Fig. 6: Iso-surface of Q-criterion with the vorticity magnitude being colored.

Loading noise is a dipole noise source dependent on the unsteady lift force experienced by the rotor blades. Therefore, BVI noise can be identified due to peaks in the normal force coefficient derivative term. Using data from OVERFLOW's EROTOR history text file, second-order central difference was applied to obtain the normal force derivative values over the course of the last revolution. Plotting the results in Fig. 7, the discrepancies are most prominent on the retreating side of the rotor disk plot between the azimuth angles of 270° and 315°.

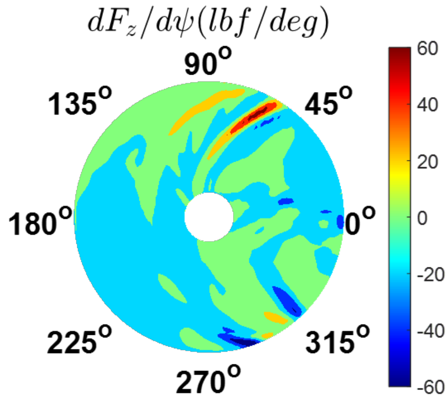

(a)

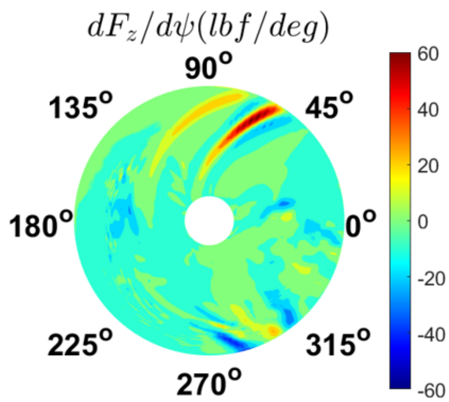

(b)

Fig. 7: Normal force derivative on the rotor disk: (a) baseline and (b) Serr_0.1_1.

Figure 8 shows the force derivative value at the 97% blade span location on the rotor blade for both the baseline and Serr_0.1_1. The serration case shows a decrease in the force derivative near the retreating side. On the advancing side, the two results are similar.

Considering the reduction in the force derivative term, the CFD results imply a significant noise reduction occurring from a less intensive loading force fluctuation.

2. BVI Acoustics

This paper mainly focuses on tonal noise or harmonics of the blade passing frequency (BPF). Although high-frequency broadband noise is important and can be affected by the installation of serrations (Refs. 19, 20), this aspect is not discussed in this paper.

Figure 9 presents the acoustic pressure over half of the rotor revolution. For the front microphone, the predictions for both

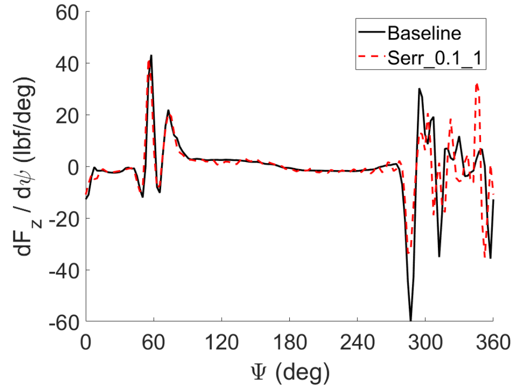

Fig. 8: Normal force derivative at 97% blade span over last revolution.

the baseline and serrated geometries are compared against experimental data. The simulations successfully capture a strong BVI event, showing good agreement with the measured data. However, the difference in acoustic response between the baseline and serrated cases is minimal for the front microphone. For the rear microphone, the serrated leading edge results in a significant reduction in noise, with nearly a 50% decrease in the BVI peak. This suggests that the serration geometry is more effective in reducing BVI noise when a direct BVI event occurs. Both the front and rear acoustic signatures share a similar shape with a negative-positive-negative peak pattern.

Figure 10 presents the SPL at both microphone locations. The BPF is 75.1 Hz. The frequency between 7th and 50th is defined as BVI frequency in this paper, which is used to filter the acoustic signatures earlier and plot the directivity later. For the front microphone, the SPL remains similar between the baseline and serrated cases up to 1,800 Hz (24th harmonic). However, beyond 1,800 Hz, the serrated case exhibits lower SPL levels. In contrast, at the rear microphone, a noticeable noise reduction is observed in the mid-frequency range between 700 Hz (9th harmonic) and 2,500 Hz (33th harmonic), while an increase in noise is evident at higher frequencies.

3. Effects of Serration Geometries

Figure 11 displays the BVI noise directivity in the vertical plane or side view, where the noise is band-filtered between the 7th and 50th harmonics of the BPF, which is defined as the range of BVISPL. The observer is located at a distance of 10 rotor radii. In the plot, 0° denotes the in-plane direction and 90° represents the position directly above the rotor. The results indicate a clear BVI noise reduction of up to 5 dB at certain rear directivities, attributed to the reduction of retreating blade BVI. As expected, the serrated leading edge proves to be most effective in the primary BVI noise propagation direction, particularly between 30° and 60° in elevation angle.

Serration geometry is varied to determine which component of the serration is responsible for the noise reduction mechanism. Adjusting the $2h/\lambda = 0.5$, Fig. 11(b), shows similar

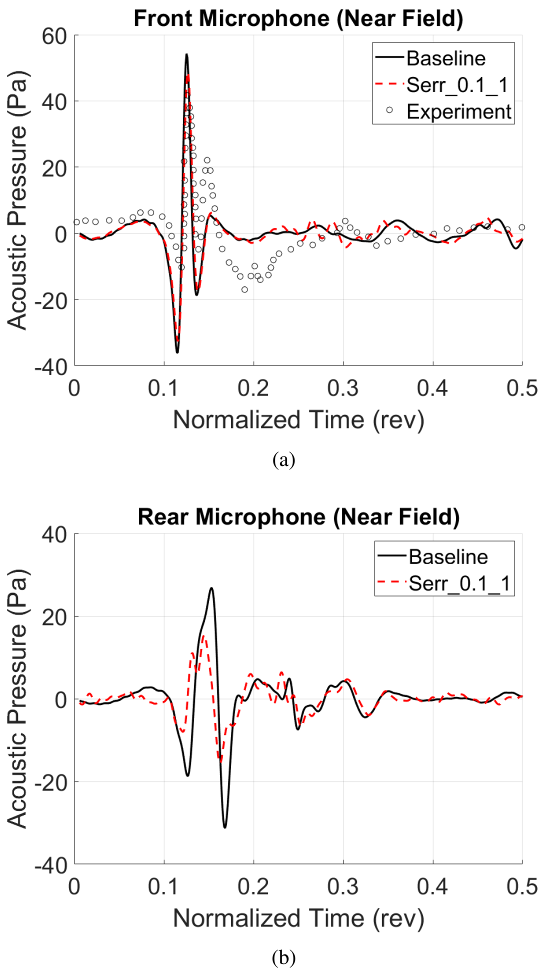

Fig. 9: Acoustic pressure of the OLS rotor with and without the serration: (a) front microphone with experimental data and (b) rear microphone.

noise reduction levels as Fig. 11(a). However, noise reduction is less noticeable with $2h/\lambda = 0.25$ in Fig. 11(c).

Sound power level (PWL) is calculated by summing up BVISPL across rear microphones. Table 4 shows the difference of PWL between the baseline and serration cases. It is shown that the maximum noise reduction occurs at $2h/c = 0.1$ and $2h/\lambda = 1$ in which about 4 dB PWL reduction is achieved. It is also found that the noise reduction is more sensitive to the height-to-wavelength ratio than height-to-chord ratio. This implies that the amount of serrations on a rotor blade is more important than the height of the serrations. Note that Serr_0.2_0.25, which has only one serration, yields an increase in PWL due to higher noise than the baseline case between 60° and 90° as well as 270° and 300°.

Table 4: Difference of PWL between baseline and serrated cases.

ΔPWL (dB)	**2h/λ = 1**	**2h/λ = 0.5**	**2h/λ = 0.25**
2h/c = 0.05	-2.9122	-2.7074	-2.0591
2h/c = 0.1	-3.9082	-2.7000	-0.9124
2h/c = 0.2	-2.0678	-2.3664	0.4798

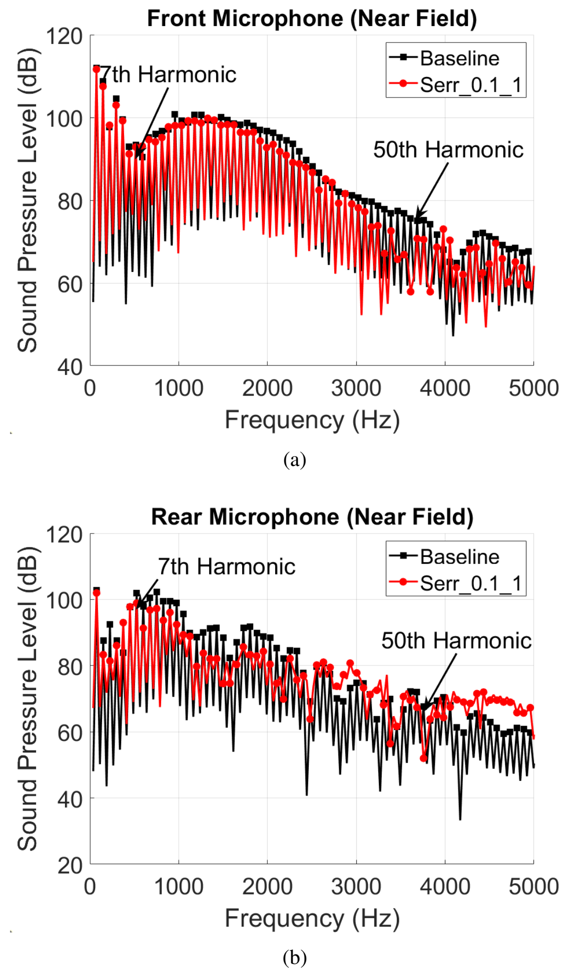

Fig. 10: Sound pressure level of the OLS rotor with and without the serration: (a) front microphone and (b) rear microphone.

Noise directivities in the far field are investigated to determine how acoustic signatures are altered by the serrated leading-edge design. Focusing on serration cases where $2h/\lambda = 1$, Fig. 12 displays SPL plots for different height-to-chord ratios of serrations at the microphones of 30°, 60°, 90°, 270°, 300°, and 330°. The difference of SPL between the baseline and serration cases identifies the frequency range in which SPL is reduced for different microphones. While the microphones of 90° and 270° show reduction across all BPF, other microphones only see significant reduction at lower frequency values. After the 30th BPF harmonic, there is an increase in SPL, implying that leading-edge serrations may increase high-frequency noise, although the magnitude is low at high frequencies.

Figure 13 shows the effect of the serration height-to-wavelength ($2h/\lambda$) ratios while keeping $2h/c = 0.1$. It is found that BVISPL directivity is sensitive to $2h/\lambda$ values, especially at the rear microphones. For instance, Serr_0.1_1 case shows noise reduction at all specified microphones up to approximately 30th harmonic. In contrast, the Serr_0.1_0.25 case does not show a clear noise decreasing trend at a wide range of harmonic numbers for each microphone. This result

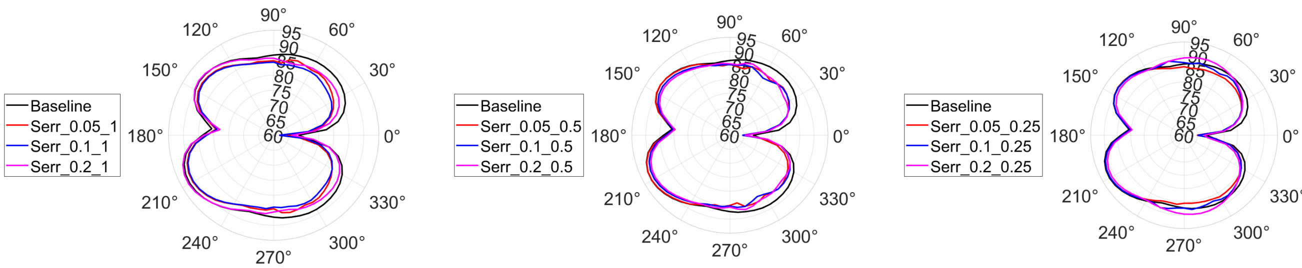

(a) (b) (c)

Fig. 11: BVISPL noise directivities between baseline and serrated cases: (a) 2h/λ = 1, (b) 2h/λ = 0.5, and (c) 2h/λ = 0.25.

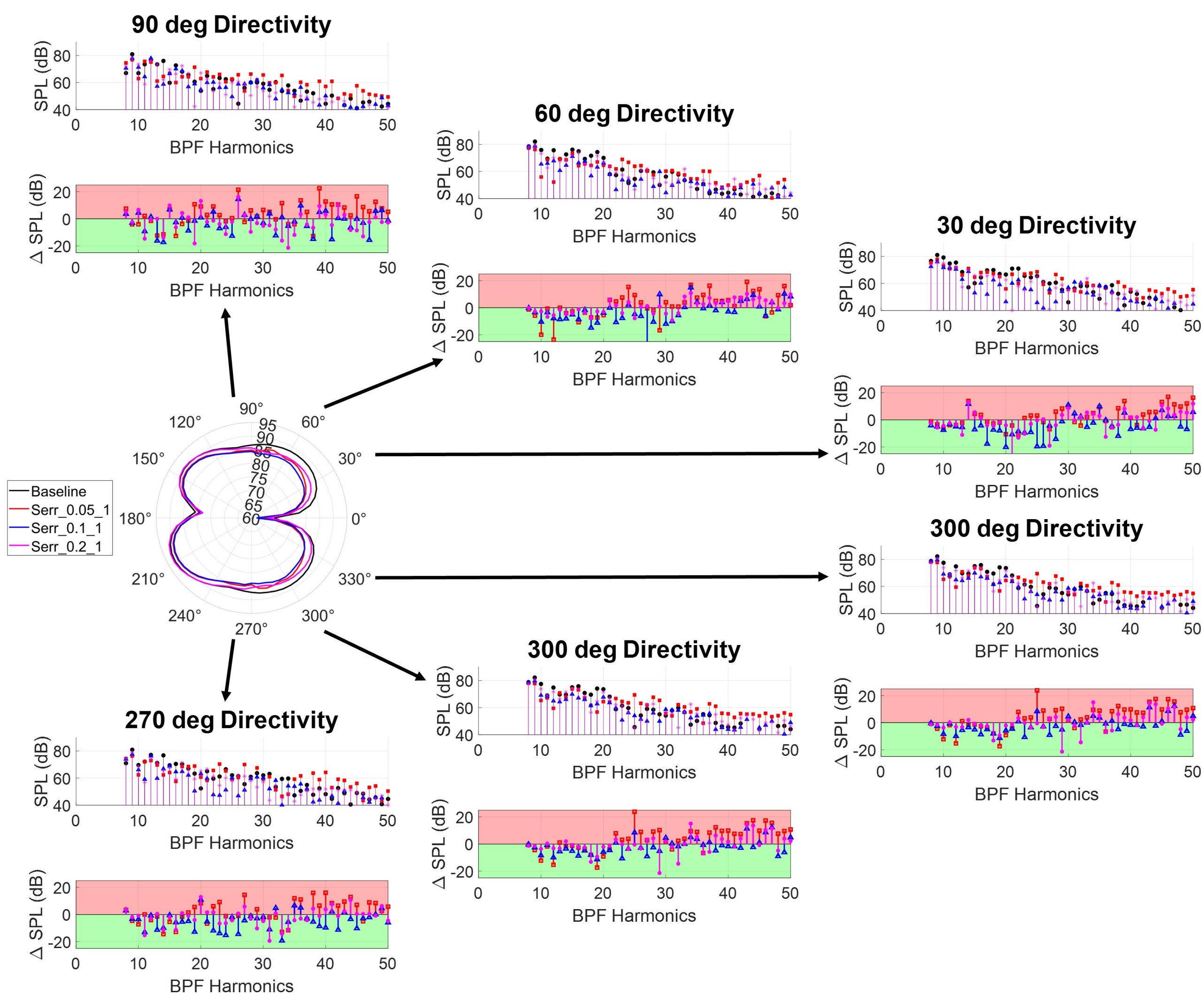

Fig. 12: Effects of 2h/c on SPL at rear microphones (2h/λ = 1).

is consistent to Table 4.

Due to the oscillating nature of a sine wave, the modified geometry of the serrated blade maintains the same planform area as the rectangular blade. As a result, the thrust coefficient in the baseline case and serrated cases are similar in value of 0.0059. However, the power coefficient varies drastically from the baseline case value of 0.00031. The thrust and power coefficients for each serrated case are determined and shown in Table 5. Negative percentages refer to a decrease in that parameter, while positive percentages refer to an increase in

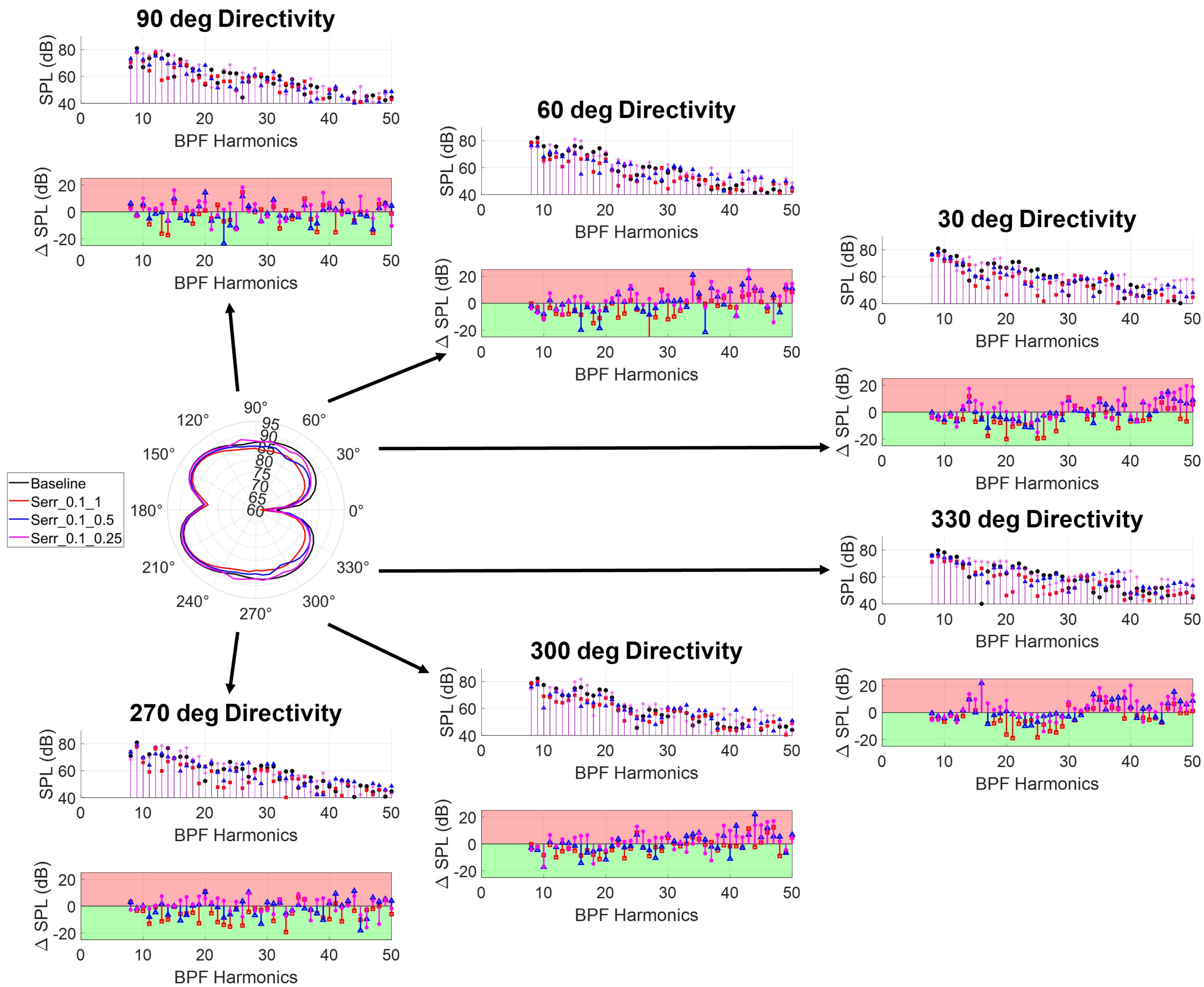

Fig. 13: Effects of 2h/λ on SPL at rear microphones (2h/c = 0.1).

that parameter. It is shown that the serration cases dramatically increase the power coefficient by about 20-30%. While leading-edge serrations can achieve BVI noise reduction, the power increase can be a significant drawback.

Table 5: Difference in thrust and power coefficient between baseline and serrated cases.

C_T	**2h/λ = 1**	**2h/λ = 0.5**	**2h/λ = 0.25**
2h/c = 0.05	-1.7%	-1.7%	-1.7%
2h/c = 0.1	-3.4%	-1.7%	-1.7%
2h/c = 0.2	-3.4%	-1.7%	-3.4%
C_P	**2h/λ = 1**	**2h/λ = 0.5**	**2h/λ = 0.25**
2h/c = 0.05	22.3%	29.8%	23.5%
2h/c = 0.1	29.6%	30.4%	26.2%
2h/c = 0.2	35.6%	30.5%	19.5%

4. Noise Source Identification

Figure 14 shows the loading noise integrand at the azimuthal angle of 238.5° for the baseline and serrated cases with $2h/\lambda = 1$. The baseline case is predominantly negative, contributing a strong negative BVI peak. Serr_0.5_1 shows slight flucatuations in loading noise sources along the blade as positive loading sources are introduced while Serr_0.1_1 and Serr_0.2_1 show extreme fluctuations in loading noise sources along the blade.

When comparing the results of all four contour plots at the 80% span, the positive and negative noise source fluctuation is captured along the chordwise direction from 20% onwards for the serrated cases. This is most likely due to the break down of vortex structures across the blade during a BVI event, generating noise sources with opposing phases. Eventually, this out-of-phase noise source characteristics promote the destructive interference of noise at the far field, reducing BVI noise.

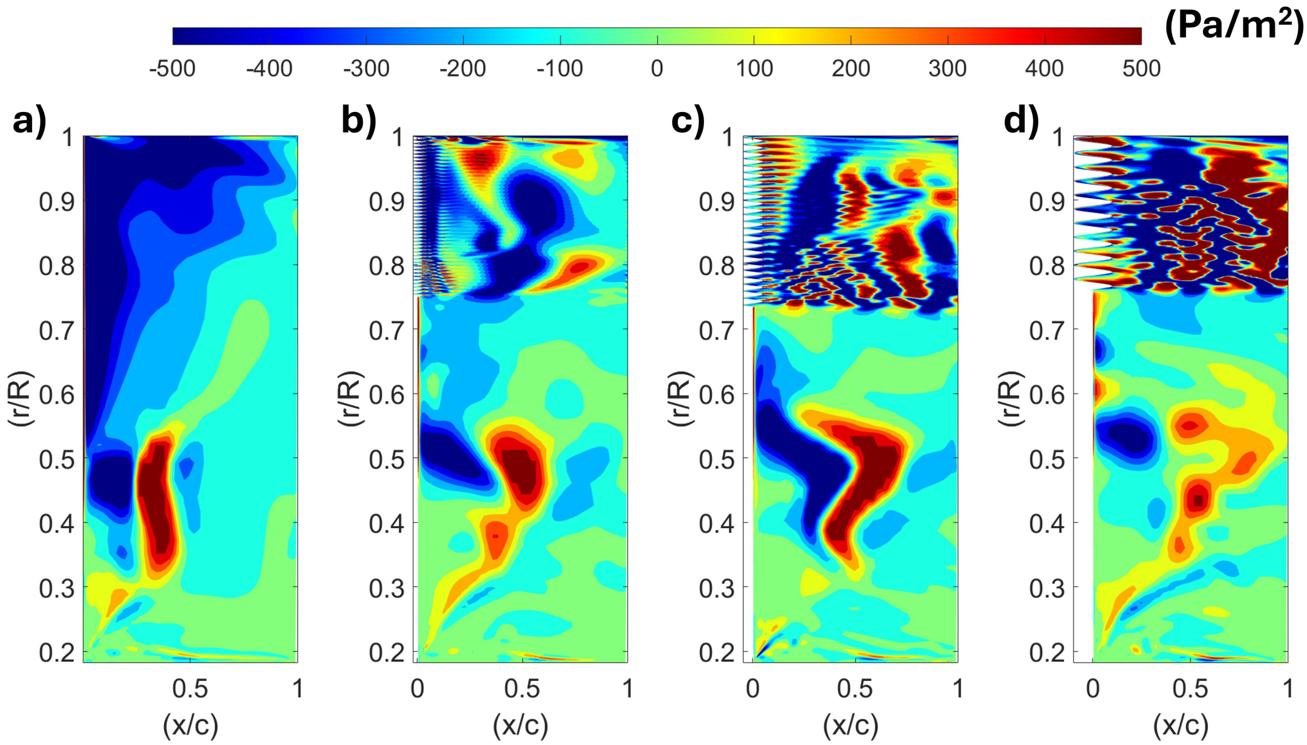

Fig. 14: Loading noise integrand contour on suction side at $\psi = 238.5°$: (a) Baseline, (b) Serr_0.05_1, (c) Serr_0.1_1, and (d) Serr_0.2_1.

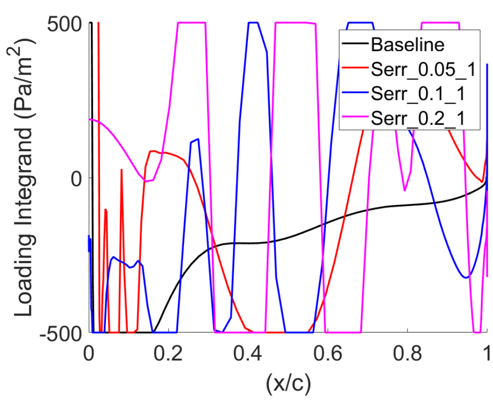

Fig. 15: Loading noise integrand at 80% blade span for baseline and serrated cases ($2h/\lambda = 1$).

CONCLUSION

High-fidelity CFD simulations demonstrated that introducing a serrated leading edge to the OLS rotor can effectively mitigate noise generated by the interaction between the rotor blade and its own vortices. Leading-edge serrations on rotor blades have been shown to effectively reduce noise by up to 5 dB of BVISPL or approximately 2–4 dB of PWL in the rear region of the aircraft. Moreover, increasing the number of serrations on the leading edge correlated with greater noise reduction. Rear directivity patterns also revealed that SPL tends to decrease at frequencies between the 7th and 30th BPF harmonics. However, while leading-edge serrations reduce noise, they come with the tradeoff of increasing the power coefficient due to increased parasitic drag. Thus, it would be desirable to configure the rotor blades so that the serrations can be deployed selectively when BVI noise reduction is a primary concern.

Interestingly, the serrations were effective only when the vortices directly impinge on the blades on the retreating side. When the tip vortices pass over the blade surface on the advancing side, no significant noise reduction was observed.

The BVI noise reduction mechanism was also investigated. First, the normal force derivative, or the source strength, was found to be reduced on the retreating side. The normal force was the integrated quantity along the chordwise direction. Second, the out-of-phase behavior of the loading noise sources in the chordwise direction contributed destructive interference of noise. It is thought that the reduction in source strength results from the out-of-phase pressure distributions. Further studies are needed to clarify the underlying physical mechanism of the noise reduction.

REFERENCES

[1]Yu, Y. H., "Rotor Blade–Vortex Interaction Noise," *Progress in Aerospace Sciences*, Vol. 36, (2), 2000, pp. 97–115.
doi: 10.1016/S0376-0421(99)00012-3

[2]Jia, Z., Lee, S., Sharma, K., and Brentner, K. S., "Aeroacoustic Analysis of a Lift-Offset Coaxial Rotor Using High-Fidelity CFD/CSD Loose Coupling Simulation," *Journal of*

the American Helicopter Society, Vol. 65, (1), 2020, pp. 1–15(15).
doi: 10.4050/JAHS.65.012011

[3]Jia, Z. and Lee, S., "Aerodynamically Induced Noise of a Lift-Offset Coaxial Rotor with Pitch Attitude in High-Speed Forward Flight," *Journal of Sound and Vibration*, Vol. 491, 2021, pp. 115737.
doi: 10.1016/j.jsv.2020.115737

[4]Jia, Z. and Lee, S., "Impulsive Loading Noise of a Lift-Offset Coaxial Rotor in High-Speed Forward Flight," *AIAA Journal*, Vol. 58, (2), 2019, pp. 687–701.
doi: 10.2514/1.J058295

[5]Posa, A., Broglia, R., Shi, W., and Felli, M., "Comparison between the Acoustic Fields of Conventional and Tubercled Propellers," *Physics of Fluids*, Vol. 37, 2025, pp. 025118.
doi: 10.1063/5.0251584

[6]Jia, Z. and Lee, S., "High-Fidelity Computational Analysis on the Noise of a Side-by-Side Hybrid VTOL Aircraft," *Journal of the American Helicopter Society*, Vol. 67, (2), 2022, pp. 1–14(14).
doi: 10.4050/JAHS.67.022005

[7]Jia, Z. and Lee, S., "Computational Study on Noise of Urban Air Mobility Quadrotor Aircraft," *Journal of the American Helicopter Society*, Vol. 67, (1), 2022, pp. 1–15(15).
doi: 10.4050/JAHS.67.012009

[8]Sagaga, J. and Lee, S., "Performance, Aerodynamics, and Aeroacoustics of Side-by-Side Rotors Using High-Fidelity Computational Fluid Dynamics," *AIAA Journal*, Vol. 61, (12), 2023, pp. 5429–5445.
doi: 10.2514/1.J062955

[9]Sagaga, J. and Lee, S., "High-Fidelity Computational Study of Aerodynamic Noise of Side-by-Side Rotor in Full Configuration," *Journal of Sound and Vibration*, Vol. 592, 2024, pp. 118607.
doi: 10.1016/j.jsv.2024.118607

[10]Ilie, M., "Active Flow Control Technique for the Reduction of Helicopter BVI Noise; a Numerical Study using LES," *48th AIAA Aerospace Sciences Meeting Including the New Horizons Forum and Aerospace Exposition*, 2010.
doi: 10.2514/6.2010-1411

[11]Wei, Y., Xu, F., Bian, S., and Kong, D., "Noise Reduction of UAV Using Biomimetic Propellers with Varied Morphologies Leading-edge Serration," *Journal of Bionic Engineering*, Vol. 17, (4), 2020, pp. 767–779.
doi: 10.1007/s42235-020-0054-z

[12]Narayanan, S., Chaitanya, P., Haeri, S., Joseph, P., Kim, J. W., and Polacsek, C., "Airfoil Noise Reductions Through Leading Edge Serrations," *Physics of Fluids*, Vol. 27, (2), 2015, pp. 025109.
doi: 10.1063/1.4907798

[13]Feinerman, J. A., Koushik, S., and Schmitz, F. H., "Effect of Leading-Edge Serrations on Helicopter Blade–Vortex Interaction Noise," *Journal of the American Helicopter Society*, Vol. 62, (3), 2017, pp. 1–11.
doi: 10.4050/JAHS.62.032001

[14]Boxwell, D. A., Schmitz, F. H., Splettstoesser, W. R., and Schultz, K. J., "Helicopter Model Rotor-Blade Vortex Interaction Impulsive Noise: Scalability and Parametric Variations," *Journal of the American Helicopter Society*, Vol. 36, (1), 1987, pp. 3–12.
doi: 10.4050/JAHS.32.1.3

[15]Lee, S., Bretner, K., Farassat, F., and Morris, P. J., "Analytic Formulation and Numerical Implementation of an Acoustic Pressure Gradient Prediction," *Journal of Sound and Vibration*, Vol. 319, (3–5), 2009, pp. 1200–1221.
doi: 10.1016/j.jsv.2008.06.028

[16]E., F. W. J. and L., H. D., "Sound Generation by Turbulence and Surfaces in Arbitrary Motion," *Philosophical Transactions of the Royal Society of London. Series A, Mathematical and Physical Sciences*, 1969, pp. 321–342.
doi: http://doi.org/10.1098/rsta.1969.0031

[17]Brentner, K. S. and Farassat, F., "Modeling Aerodynamically Generated Sound of Helicopter Rotors," *Progress in Aerospace Sciences*, Vol. 39, (2), 2003, pp. 83–120.
doi: https://doi.org/10.1016/S0376-0421(02)00068-4

[18]Farassat, F. and Succi, G., "The Prediction of Helicopter Rotor Discrete Frequency Noise," *VERTICA*, Vol. 7, (4), 1983, pp. 309 – 320.

[19]Lee, S., Ayton, L., Bertagnolio, F., Moreau, S., Chong, T. P., and Joseph, P., "Turbulent Boundary Layer Trailing-Edge Noise: Theory, Computation, Experiment, and Application," *Progress in Aerospace Sciences*, Vol. 126, 2021, pp. 100737.
doi: 10.1016/j.paerosci.2021.100737

[20]Li, S. and Lee, S., "Analytic Prediction of Rotor Broadband Noise with Serrated Trailing Edges with Applications to Urban Air Mobility Aircraft," *Journal of the American Helicopter Society*, Vol. 69, 2024, pp. 032005.
doi: 10.4050/JAHS.69.032005